Chandler wobble and pole tide in relation to interannual atmosphere-ocean dynamics

Hans-Peter Plag

Institut für Geophysik, Christian-Albrechts-Universität zu Kiel, Olshausenstr. 40, D-24118 Kiel, Germany

Abstract. Since the discovery of the Chandler wobble in polar motion more than a century ago, the cause of the wobble remained obscure. As long as one assumes the observed wobble to be a free damped mode of the rotating Earth, a reoccurring excitation of the wobble has to be assumed likewise. Neither the cause and mechanism of this excitation nor the damping of the wobble have satisfactorily been explained. Furthermore, the analyses of polar motion data under the above assumption lead to contradictory results, namely (1) a multi-frequency or a single frequency wobble, (2) an amplitude-dependent frequency, (3) a large diversity of Q-values.

A detailed study of polar motion, oceanographic, and meteorological data gave rise to the hypothesis that the observed wobble in fact is a forced oscillation, with a slightly variable forcing frequency. The consequences of this hypothesis are discussed. A possible forcing mechanism is found in a large-scale, quasi-periodic variation in air pressure within the Chandler band. This fourteen–to–sixteen months atmospheric fluctuation is responsible for most of the oceanic pole tide hitherto attributed to the Chandler wobble, and it is the most prominent candidate for forcing the observed wobble.

Regarding the observed Chandler wobble as a forced resonant phenomenon and not as a purely free wobble raises the question of the true Chandler period and the wobble Q. However, the determination of both, period and Q, is strongly limited by the amount of available data and the still unknown amplitude of the forcing function.

1 Introduction

For a body rotating about its axis of the main moment of inertia a suitable excitation may result in a displacement of the figure axis with respect to the rotation axis. The analysis of the equation of rotation of a rigid body with rotational symmetry reveals that for such a displacement exactly one eigenmode exists, i.e., after excitation, the figure axis oscillates around the rotation axis with this oscillation commonly being denoted as wobble. The path of the instantaneous rotation axis $\mathbf{p}(t)$ at the surface of the body with respect to an arbitrary point $\mathbf{p}_0$ close to the figure axis, i.e., the path $\hat{\mathbf{p}}(t) = \mathbf{p}(t) - \mathbf{p}_0$ is usually considered as polar motion (PM).

Of course, the rotation axis may also move in space. For the Earth's rotation, these motions are known as precession and nutation (see, e.g. Munk and

MacDonald, 1960). Here the motion of the rotation axis in space will not be considered and the discussion will be restricted to PM.

Already Euler had shown that the period of the free wobble depends on the angular velocity and the main moments of inertia of the rotating body. Taking the Earth as a rigid body, Euler found the resulting eigenperiod to be 305 days or approximately 10 months. For an observer at the Earth's surface, PM results in latitude variations and in variations of the siderial time. In the nineteenth century, when latitude observations became available with sufficient precision, Euler's results stimulated an extensive search for the wobble in these observations.

A peculiar controversy started at the end of the last century between S. C. Chandler and several theoreticians. Chandler, who analyzed observations of PM without having any preconceptions concerning the period of the free Eulerian nutation found this period to be about 427 days (approx. 14 months) instead of the expected Eulerian period of 305 days (or about ten months) (Chandler, 1891). Furthermore, his results indicated a variable wobble period (Chandler, 1892, 1893), and in 1902 he published his 'inverse relation between angular velocity and radius' (Chandler, 1902). Theoreticians including Newcomb rejected these results when first published defending the 'laws of dynamics' (see Mulholland and Carter, 1982, for a more detailed discussion of this controversy). The period of the wobble was accepted only after Newcomb's – partly wrong – explanation, but the latter results continuously are a matter of discussion.

Today, a century later, the controversy still is not resolved, and the interpretation of the observed Chandler wobble (CW) continues to depend mainly on the various preconceptions of the different authors. Analyzing the most advanced of the long polar PM series, both, the annual and Chandler wobbles turn out to have variable amplitudes (Chandler, 1902), and, while the instantaneous frequency and phase of the annual wobble (AW) are nearly fixed, the respective parameters of the CW exhibit considerable temporal fluctuations (Guinot, 1982). The relationship between the instantaneous CW amplitude and frequency already detected by Chandler (1902) has been confirmed for the subsequent data, too (Vondràk, 1985). On the other hand, the spectra of the long series exhibit multiple Chandler peaks with at least two distinct main peaks. Depending on the authors' preconceptions, most of these aspects of the observed CW were attributed to data errors or inhomogeneities (Lambeck, 1980; Lenhardt and Groten, 1985), to a multiple-frequency CW (Ooe, 1978; Dickman, 1981; Chao, 1983), a frequency-modulated wobble (Carter, 1981), non-linear effects (Vondràk, 1985), or multiple excitations (Plag, 1988). However, up to now, besides dismissing the observations as being erroneous, no physically sound explanation of the observed characteristics or the proposed nature of the CW has been given.

Since the discovery of the CW, there has been an ongoing discussion concerning the origin of this wobble. The CW observed in the polar motion data with a period of nearly fourteen months commonly has been considered as the damped free rotational mode of the rotating, viscoelastic Earth with oceans and

continents, corresponding to the ten months Eulerian period of a rigid, oceanless Earth. Due to the damping, the wobble should die out after a certain period of time elapsed since the last excitation. Since observations tell us, that the wobble is not dying out but rather exhibiting increasing amplitudes at times, it has been assumed that there are sources frequently exciting the wobble anew. The problem of the CW excitation has been attacked in a large number of papers, and earthquakes (Smylie and Mansinha, 1971; Kanamori, 1976; Mansinha *et al.*, 1979; Souriau, A., 1986; Gross, 1986; Maddox, 1988; Preisig, 1992) and the atmosphere (e.g. Wilson and Haubrich, 1976b,a; Merriam, 1982; Barnes *et al.*, 1983; Hide, 1984) have been considered as possible causes for the excitation of the wobble (see Runcorn *et al.*, 1988, for a comprehensive review). However, according to our current knowledge, the displacements due to earthquakes and the associated changes in the moment of inertia are an order of magnitude too small to account for the observed wobble amplitude. Using the polar motion equations for a viscoelastic Earth with non-global oceans, Pejovič and Vondrák (1991) could show that a large part of the wobble may be due to atmospheric forcing. Nevertheless, there remain considerable discrepancies between model predictions and the observed polar motion.

In the last two decades, several long series of polar motion became available. For the present study, which depends strongly on the temporal variations of the observed wobbles, it is of importance to select the most homogeneous of the available series. Therefore, in Appendix A the different data sets are compared with each other, using the geometric properties of the pole path to discuss data homogeneity and the smoothness of the path. Based on the material compiled in this appendix, it is concluded that the series provided by Yumi and Yokoyama (1980; denoted as YY) are the most homogeneous ones.

In the following section, a short introduction to the theory of PM is given, which is used to simulate PM forced by atmospheric excitation. In section 3, the – largely well known – characteristics of the CW as determined from the YY-series are discussed. These characteristics are essential for the hypothesis concerning the nature of the observed wobble put forward in section 4. Based on this new hypothesis, sections 5 and 6 introduce the oceanic and atmospheric phenomena which potentially may force the CW in PM. In section 7, the equations for PM of a simple Earth model are used to predict PM for atmospheric excitations constructed from observations. The characteristics of the CW in the predicted PM are then compared to those of the observed CW. The main conclusions are summarized and discussed in section 8. Finally, in an appendix the available different PM series are critically assess with respect to their aptitude for studies of the characteristics of PM at interannual time scales.

2 Theory of polar motion

In general, there are two principle ways of modeling polar motion due to angular momentum exchange between the Earth's mantle and the core, atmosphere and oceans: (1) based on the momentum balance, deformations of the Earth due to

the momentum and pressure forcing on the mantle are calculated and the mean vorticity of the surface deformations is used to determine polar motion, and (2) based on the angular momentum balance equations for the rotation vector are derived and solved for given excitations due to, for example, the atmosphere (for a more detailed description of the advantages and problems of these approaches see, for example Lambeck, 1988).

Only the second approach will be considered here. The angular momentum balance is given as

$$\frac{d}{dt}\mathbf{H} = \mathbf{L}, \tag{1}$$

with $\mathbf{H}$ the total angular momentum of the body, and $\mathbf{L}$ the external torque in an inertial frame of reference. Transforming this balance into a reference frame rotating with $\boldsymbol{\Omega}(t)$ results in

$$\mathbf{H} = \boldsymbol{\Theta} \cdot \boldsymbol{\Omega} + \mathbf{h}, \tag{2}$$

where $\mathbf{h}$ is the relative angular momentum of the body, and $\boldsymbol{\Theta}$ is the (time-dependent) inertia tensor defined as

$$\boldsymbol{\Theta}(t) = \int_{V(t)} \rho(\mathbf{x}, t)(\mathbf{x}^2 \boldsymbol{I} - \mathbf{x} \otimes \mathbf{x}) dV \tag{3}$$

($\mathbf{x} \otimes \mathbf{x}$ results in a tensor with components $c_{ij} = x_i x_j$). In a reference frame rotating with angular velocity $\boldsymbol{\Omega}$ relative to the inertial frame, the angular momentum balance is written as

$$\boldsymbol{\Omega} \times (\boldsymbol{\Theta} \cdot \boldsymbol{\Omega} + \mathbf{h}) + \dot{\mathbf{h}} + \frac{d}{dt}(\boldsymbol{\Theta} \cdot \boldsymbol{\Omega}) = \mathbf{L}. \tag{4}$$

This equation is non-linear in $\boldsymbol{\Omega}$ and describes the global rotation of an arbitrary body. In general, the external torque $\mathbf{L}$, the total angular momentum $\mathbf{H}$, the relative angular momentum $\mathbf{h}$ and the inertia tensor $\boldsymbol{\Theta}$ are all time-dependent parameters.

In literature, different special cases are used for $\boldsymbol{\Omega}$, and the case $\boldsymbol{\Omega} = \boldsymbol{\Omega}_0 =$ const. is emphasized here (see e.g. Smith, 1977). Selecting a uniformly rotating reference frame (sometimes called the nutation system) has several advantages but also disadvantages, and the latter motivate the use of a reference frame fixed to the rotating body.

For a nearly constant angular speed, a perturbation approach with

$$\boldsymbol{\Omega}(t) = \Omega_0(\mathbf{e}_z + \mathbf{m}(t)) = (m_1(t), m_2(t), 1 + m_3(t))^t \Omega_0 \tag{5}$$

$$\mathbf{H}(t) = \boldsymbol{\Theta}(t) \cdot \boldsymbol{\Omega}(t) + \mathbf{h}(t) \tag{6}$$

$$\boldsymbol{\Theta}(t) = \boldsymbol{\Theta}_0 + \boldsymbol{c}(t), \tag{7}$$

where m_i, h_i and c_{ij} are small in first order, can be used to rewrite the system of equations (4). The coordinate axes are aligned with the main axes of the moment of inertia tensor, i.e., this tensor is given as

$$\boldsymbol{\Theta}_0 = \begin{pmatrix} A & 0 & 0 \\ 0 & B & 0 \\ 0 & 0 & C \end{pmatrix}. \tag{8}$$

Dropping all terms of order higher than one in system (4) leads to the Euler-Liouville-equations (ELE)

$$\begin{aligned} \boldsymbol{\Omega}_0 \times \mathbf{h} + \Omega_0 \boldsymbol{\Omega}_0 \times (\boldsymbol{\Theta}_0 \cdot \mathbf{m}) + \Omega_0 \mathbf{m} \times (\boldsymbol{\Theta}_0 \cdot \boldsymbol{\Omega}_0) + \\ \boldsymbol{\Omega}_0 \times (\boldsymbol{c} \cdot \boldsymbol{\Omega}_0) + \dot{\mathbf{h}} + \Omega_0 \boldsymbol{\Theta}_0 \cdot \dot{\mathbf{m}} + \dot{\boldsymbol{c}} \cdot \boldsymbol{\Omega}_0 = \mathbf{L}, \end{aligned} \tag{9}$$

where the dotted quantities indicate their derivatives with respect to time. Assuming rotational symmetry (i.e., $A = B$), introducing the complex quantities

$$\begin{aligned} m &= m_1 + i m_2 \\ c &= c_{13} + i c_{23} \\ h &= h_1 + i h_2 \\ L &= L_1 + i L_2 \end{aligned} \tag{10}$$

and defining the excitation functions

$$\Psi^{\mathrm{PM}} = \frac{-1}{\Omega_0^2 (C - A)} (\Omega_0 \dot{c} + i \Omega_0^2 c + \dot{h} + i \Omega_0 h - L) \tag{11}$$

$$\Psi^{\mathrm{LOD}} = \frac{-1}{\Omega_0 C} (\Omega_0 c_{33} + h_3 - L_3), \tag{12}$$

results in the final form of the linear equations for PM and length-of-day (LOD) changes, i.e.

$$\frac{\dot{m}}{\sigma_r} - i m = \Psi^{\mathrm{PM}} \tag{13}$$

$$\dot{m}_3 = \dot{\Psi}^{\mathrm{LOD}}, \tag{14}$$

where the wobble frequency σ_r is given by

$$\sigma_r = \Omega \frac{(C - A)}{A}. \tag{15}$$

For a rigid body with $\dot{\boldsymbol{\Theta}} = 0$ and in a body-fixed reference frame (i.e. $\mathbf{h} = 0$), the excitation functions (11) and (12) in the absence of external torque $\mathbf{L}$ reduce to

$$\Psi^{\mathrm{PM}} = \frac{-1}{\Omega_0^2 (C - A)} (\Omega_0 \dot{c} + i \Omega_0^2 c) \tag{16}$$

$$\Psi^{\mathrm{LOD}} = \frac{-1}{C} (c_{33}). \tag{17}$$

The ELE given in (13) and (14) show that in the linearized case PM and LOD changes are decoupled. For polar motion, the equations describe a linear oscillator, while LOD changes can be computed directly by integration of the respective excitation function over time.

Strictly speaking, the ELE describe the rotation of the Earth without a core. Is, in general, the body separable into layers which may rotate with respect

to each other, then for each layer the angular momentum balance has to be considered, i.e.

$$\boldsymbol{\Omega} \times \sum_{i=1}^{n} \mathbf{H}^i + \frac{d}{dt} \sum_{i=1}^{n} \mathbf{H}^i = \mathbf{L} \tag{18}$$

$$\boldsymbol{\Omega} \times \mathbf{H}^i + \frac{d}{dt} \mathbf{H}^i = \mathbf{K}^i \ , \ i = 1, \ldots, n-1$$

where $\mathbf{H}^i$ is the angular momentum of the i-th layer and $\mathbf{K}^i$ the torque acting on that layer, which depends on the coupling between the layers. It should be mentioned here, that for a simple Earth model with a mantle and a fluid core, the expression for σ_r has to be changed to

$$\sigma_r = \Omega_0 \frac{C_{\mathrm{M}} - A_{\mathrm{M}}}{A_{\mathrm{M}}}, \tag{19}$$

where the index M indicates that the moments of inertia for the mantle alone have to be used.

For the Earth system, a variety of geophysical effects contributes to the excitation functions through changes in the tensor of the inertia tensor or changes of the relative angular momentum. Examples are the (visco)-elastic deformations of the Earth due to changes in the Earth's rotation, influences of the oceans, atmosphere, terrestrial hydrosphere and cryosphere. The deformations of the Earth result in changes of the inertia tensor. These deformations may result from internal mass movements (earthquakes, convection) or can be due to exogenic forces such as tides or surface loads. The viscoelastic properties of the mantle as well as the various couplings to the other system constituents (inner and outer core, ocean, atmosphere) may influence the wobble period to a large extent. Thus, the elastic response of the Earth's mantle to PM changes the wobble period from 305 days to 445 days (see, e.g. Lambeck, 1980). Other important effects affecting the wobble period are due to the ocean's response to PM (shortening) and the viscous response of the mantle to PM (lengthening). The latter effect also leads to a damping of the wobble. Finally, it should be mentioned that additional layers in the system not only affect the period of the CW but also give rise to additional wobbles.

The influence of the atmosphere (and likewise hydrosphere and cryosphere) on the rotation of the Earth could be described by the torque between atmosphere and the solid Earth. However, the torque is difficult to model as it not only depends on the relative wind speed but also on, for example, the surface roughness, vegetation, and topography. Therefore, in most PM model studies, the total angular momentum of the Earth system is considered to be constant (i.e. no external torque, thus excluding body and ocean tides), and in that case, changes in angular momentum of the atmosphere have to be compensated by changes in the other layers. The present-day changes in angular momentum of the atmosphere can be calculated from observational data. It is generally assumed, that the angular momentum exchange between atmosphere and ocean is small compared to that between atmosphere and solid Earth. Separating the

angular momentum into an atmospheric part $\mathbf{H}_A$, and a solid Earth part $\mathbf{H}_E$ and doing the same for the excitation functions leads to

$$\mathbf{H} = \mathbf{H}_{\mathrm{E}} + \mathbf{H}_{\mathrm{A}} \tag{20}$$

$$\Psi^{\mathrm{PM}} = \Psi_{\mathrm{E}}^{\mathrm{PM}} + \Psi_{\mathrm{A}}^{\mathrm{PM}} \tag{21}$$

$$\Psi^{\mathrm{LOD}} = \Psi_{\mathrm{E}}^{\mathrm{LOD}} + \Psi_{\mathrm{A}}^{\mathrm{LOD}}. \tag{22}$$

Barnes *et al.* (1983) derive approximations for Ψ_{A}, which express these excitation functions in terms of the wind and surface pressure fields. However, they combine the angular momentum change of the atmosphere and the deformations of the Earth due to atmospheric loading to "Atmospheric Angular Momentum Functions (AAMF)", which is not desirable since the latter are depending on the Earth model while the first is not.

In section 7 the ELE for a layered Earth are used to simulate the PM due to atmospheric excitation for the last 100 years. These model predictions will be compared to observations in order to see whether the predicted PM exhibits the same properties as those of the observed PM described in the next section.

3 Properties of the observed Chandler wobble

The spectrum of PM has been discussed in a number of studies (e.g. Carter, 1981; Dickman, 1981; Lambeck, 1980; Chao, 1983; Lenhardt and Groten, 1985; Gross, 1985; Plag, 1988), and the basic features will be summarized. The most dominant peaks in the spectrum are those due to CW and AW (Fig. 1). The only peak in the retrograde part of the spectrum is the small peak in the amplitudes at the annual frequency, which, however, does not contribute significantly to the variance, as is seen clearly in the variance spectrum. In the prograde part, the annual and Chandler peaks provide the maximum contribution to the variance, while the contribution of the interdecadal peaks again is negligible. In the prograde Chandler band, there are several peaks present. Depending on the approach, the variations in this band have been modeled by one (Lenhardt and Groten, 1985), two (Colombo and Shapiro, 1968), three (Carter, 1981), or four harmonic constituents (Gaposchkin, 1972). Using autoregressive processes, Chao (1983) confirmed the results of Gaposchkin, while Plag (1988) found five harmonic constituents to be qualified for modeling the Chandler band. The values of Q determined in various studies of the YY series also cover a wide range between 20 and 600 (see Tab. 1), and Chao (1983) even finds two of the constituents to be characterized by negative Q values. Taking up an idea of Colombo and Shapiro (1968), Chao explains the multiple peak structure with the existence of non-elastic layers in the Earth (such as the hydrosphere, asthenosphere and outer core) and their coupling with the (visco)-elastic spheres of the Earth.

As was mentioned in the introduction, already Chandler noticed the variable amplitude of both, CW and AW, and a variable CW period. Contrary to what Chandler found from the early data, the YY series clearly demonstrate that the AW is far more stable in time than the CW (Fig. 2). However, the probably most

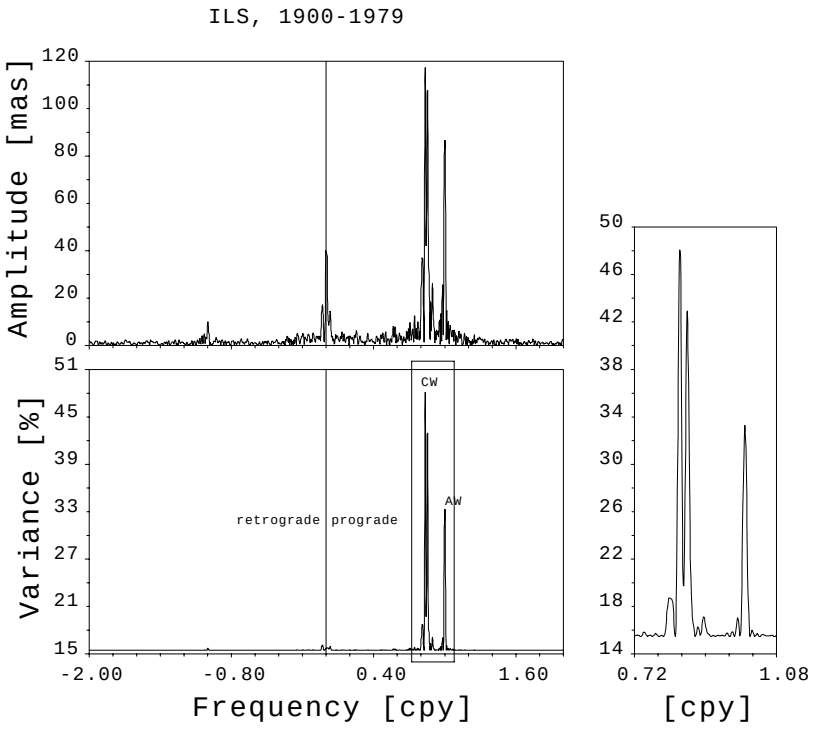

Fig. 1. Spectrum of polar motion.

Lower diagram: variance spectrum, upper diagram: corresponding amplitude spectrum. The smaller diagram to the right is enlarging the prograde Chandler to annual band of the variance spectrum. Amplitudes are given in milli-seconds of arc (mas). The variance spectrum of the ILS/IPMS series is calculated by using a circular motion with variable frequency as base function. The spectrum is defined according to an extended version (Plag, 1988) of the simple variance spectrum (Vanicek, P., 1970): Let $\mathbf{X} = \mathbf{x}(t_i),\ i = 1, \ldots, N$ be a not necessarily equidistant vector time series, with the variance $v(\mathbf{X})$ being defined in the usual way, i.e. $v(\mathbf{X}) = 1/(N-1)\sum_{i=1}^{N} \|\mathbf{x}(t_i) - <\mathbf{X}>\|$, where $<\mathbf{X}>$ is the vector of the arithmetic mean values of all $\mathbf{x}(t_i),\ i = 1, \ldots, N$. For a frequency-dependent base function $\mathbf{Y}_\omega = \mathbf{y}_\omega(t, \mathbf{p}(\omega))$ which is linear in $\mathbf{p}$, $\mathbf{p}(\omega)$ may be calculated for any value of ω, using a least squares fit of $\mathbf{Y}$ to $\mathbf{X}$. With the residual $\mathbf{R}_\omega = \mathbf{X} - \mathbf{Y}_\omega$, the variance spectrum $V\{\mathbf{X}\}$ is defined as $V\{\mathbf{X}\}(\omega) = (1 - v(\mathbf{R}_\omega)/v(\mathbf{X}))$. Here, $V\{\mathbf{X}\}$ is given in per cent. The spectra shown use the base function $\mathbf{y}_\omega(t, \mathbf{p}(\omega)) = (a\cos(\omega t) + b\sin(\omega t) + c_x + d_x t, -a\sin(\omega t) + b\cos(\omega t) + c_y + d_y t)$ with $\mathbf{p}(\omega) = (a(\omega), b(\omega), c_x(\omega), d_x(\omega), c_y(\omega), d_y(\omega))$, which is a harmonic rotation with additional trends in both components. $V\{\mathbf{X}\}$ may be estimated for any value of ω within the interval $[1/(2(t_N - t_1)), 1/\overline{\delta t}]$, where $\overline{\delta t}$ denotes the mean sampling interval.

Table 1. Some selected previous results for CW parameters.

Reference	Main conclusions
Colombo and Shapiro (1968)	Double peak structure from ILS data
Gaposchkin (1972)	Four peaks in the Chandler band
Guinot (1972)	Temporal variations in period, amplitude, and phase
Currie, Robert G. (1974)	One broad peak in ILS/IPMS data, $T_w = 432.95 \pm 1.02$ d, $Q_w = 36 \pm 10$
Graber (1976)	One peak with $T_w = 430.8$ d, $Q_w = 600$ from 15 yrs of IPMS data
Ooe (1978)	One peak with $T_0 = 0.8400 \pm 0.0039$ cpy and $50 < Q_w < 300$
Wilson and Vicente (1980)	Best estimates of $T_0 = 0.843$ cpy and $Q_w = 170$
Carter (1981)	Temporal variability attributed to frequency modulation due to solid Earth/ocean interaction
Okubo (1982)	Stable Chandler period, $50 < Q_w < 100$
Chao (1983)	Two major and two minor constituents in the YY series, Q ranging from -1930 to $+700$
Vondràk (1985)	Non-linear relationship between frequency and amplitude
Lenhardt and Groten (1985)	Several different models for the Chandler peak, Q is estimated to be as low as 24
Wilson and Vicente (1990)	CW period of 433.0 ± 1.1 days and $Q = 179$ with a range of 74 to 789
Kuehne *et al.* (1996)	CW frequency/period of 0.831 ± 0.004 cpy/439.5 ± 1.2 days
Furuya and Chao (1996)	CW period of 433.7 ± 1.8 days and $Q = 49$ with a range from 35 to 100

controversial feature of the CW in the time is the large shift of the instantaneous phase of this wobble between 1925 and 1945 (Guinot, 1972; Vondràk, 1985). This phase shift has been attributed to the double or multiple peak structure in the CW band, and, vice-versa, the multi-peaks have been attributed to the phase shift (see e.g. Dickman, 1981). In the latter case, the phase shift would be due to a hitherto unmodeled excitation process.

Already in 1902, Chandler postulated an inverse relationship between amplitude and period. This notion was taken up again by Carter (1981), who found a linear increase in the period for a decreasing CW amplitude, which he attributed tentatively to a non-equilibrium pole tide. Vondràk (1985) determined the instantaneous amplitude, period and phase of the CW (which are essentially the same as in Fig. 2). Fitting several functional relationships to amplitudes and periods, he obtained the best fit for the reciprocal dependence

$$f = 0.816 + \frac{0.0037}{a} \tag{23}$$

where f is the frequency in cpy, and a the total amplitude of the PM in arcseconds.

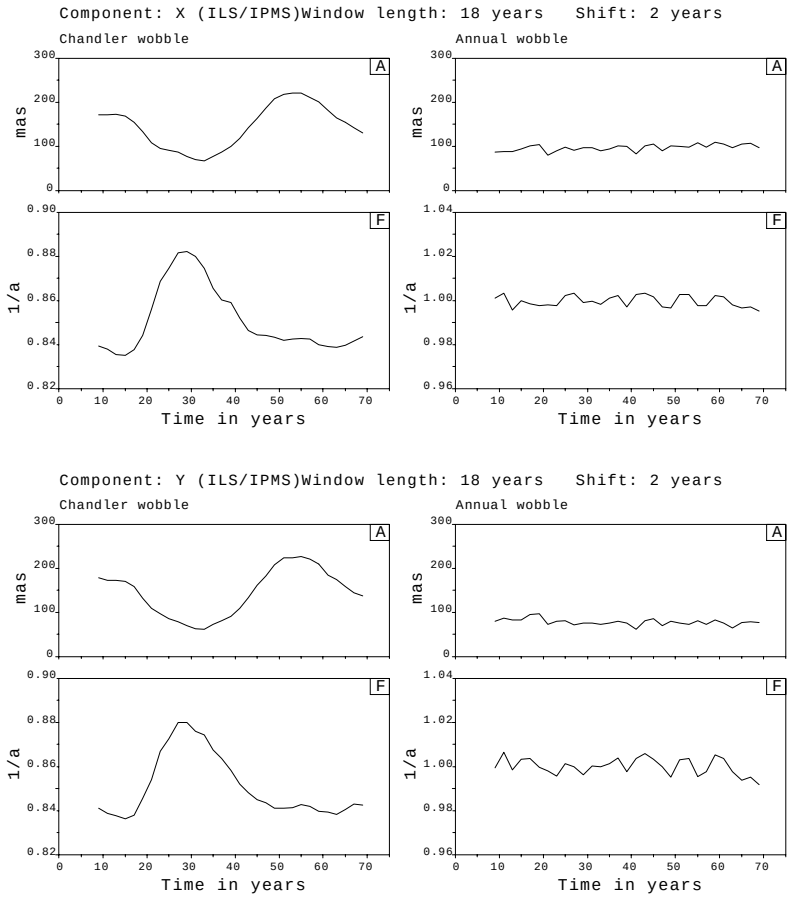

Fig. 2. Instantaneous amplitudes and frequencies of the wobbles in polar motiom.

The instantaneous CW and AW parameters are separately calculated for X- and Y-components from a fit of a model function to a moving data window. The model function comprises an AW, a CW, and the frequencies are iteratively determined. The window length is 18 years. Compare also to Plag (1988), who used a window length of 25 years, and to Vondràk (1985), who kept the annual frequency constant. A is amplitude, F frequency of the wobble.

In all the discussions during the last thirty years, the AW and the CW have been considered to be a forced motion and a free mode, respectively. Specifically, the observed CW is treated as a continuously or at least frequently excited, damped harmonic oscillation. This notion leads, of course, to discuss the period of the CW as function of amplitude, a notion which had already been dismissed by Newcomb (1891) as contradicting the 'laws of dynamics'. Nevertheless, such

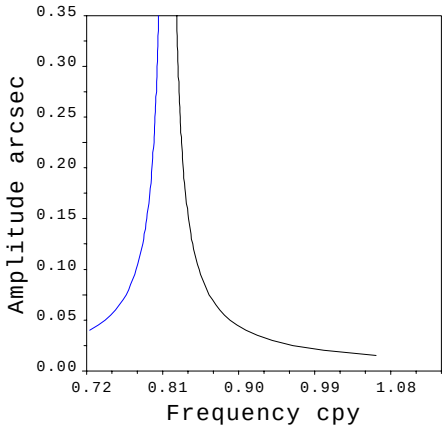

Fig. 3. Chandler wobble amplitude as function of frequency.

The functional relationships shown is the inversion of the relation $f = 0.816 + 0.0037/a$, which expresses the CW frequency f as a function of the CW amplitude a (f in cycles per year, a in seconds of arc). Vondràk (1985) found this relation to fit the pairs of instantaneous amplitude and frequencies best. Note, that Vondrák claimed non-linear effects as a cause for the dependency of the free wobble's frequency on amplitude. The inverted relation shown here, however, is strikingly similar to a resonant response to a forcing with variable frequency.

a dependence may result from some strong non-linear effects in the rotational dynamics of the real Earth. However, up to now, no evidence has been provided for non-linearity of the solid Earth's rotation. Therefore, one may ask for the consequences of dropping the notion that the observed CW includes a significant free damped contribution. In this case, the observed CW would be a forced motion, too. Particularly in the presence of a nearby resonance frequency (i.e. the Chandler frequency), we could expect the instantaneous amplitude of the wobble to be a pronounced function of the forcing frequency. Therefore, the best-fit functional given by Vondràk (1985) has been inverted and plotted in Fig. 3. The resemblance of the curve to a resonance curve is striking. Thus, the amplitude-frequency relation of the observed CW is in agreement with a resonance curve of a damped forced oscillation.

4 A new hypothesis: the observed Chandler wobble is a resonant forced oscillation

The theoretical obstacles in explaining an amplitude-dependent Chandler period, which would indicate a highly non-linear system have been discussed in the previous section. In the presence of a resonance frequency, it is more obvious to

interpret the results presented in the previous section as a frequency-dependent amplitude, instead. Thus, the observed CW may well be a forced motion instead of a freely decaying wobble. To state this hypothesis explicitly: *'The observed quasi-periodic oscillation in the pole position with a mean period of approximately 14 months is a forced, quasi-periodic motion close to a resonance period.'*

If this hypothesis is correct, it would require a quasi-periodic forcing mechanism to maintain the observed wobble. The discussion of possible candidates and forcing mechanism will be postponed until the next sections. Here, it will first be tested whether the hypothesis is capable of explaining the observed features of PM in the 14 months period band. Forced oscillation of a damped harmonic oscillator are described by the (one-dimensional) differential equation

$$\ddot{z} + \omega_0 Q^{-1} \dot{z} + \omega_0^2 z = A_0 e^{i\omega t}. \tag{24}$$

The stationary part of the solution is given by

$$z_s(t) = A(\omega) e^{i\omega t} \tag{25}$$

with the frequency-dependent amplitude $A(\omega)$,

$$A(\omega) = \frac{A_0(\omega)}{\sqrt{(\omega_0^2 - \omega^2)^2 + \omega^2 \omega_0^2 Q^{-2}}}, \tag{26}$$

where $\omega_0 = 2\pi/T_0$ and T_0 is the resonance period. For a known forcing $A_0(\omega)$, the parameters T_0 and Q of the free wobble can be estimated by fitting the base function (26) to the instantaneous CW amplitude as function of the instantaneous CW frequency, i.e. to $A_{CW}(\omega)$. However, no knowledge of the amplitude A_0 of the quasi-periodic forcing is yet available. Therefore, $A_0(\omega)$ is assumed to be constant, and the reasonability of the assumption will be discussed below.

$A_{CW}(\omega)$ is determined by iteratively fitting a base function

$$f(t) = a_1 \sin(\omega_1 t) + b_1 \cos(\omega_1 t) + a_2 \sin(\omega_2 t) + b_2 \cos(\omega_2 t) + c \tag{27}$$

to a moving data window, using the start values of 2π yr^{-1} and $2\pi/1.19$ yr^{-1} for ω_1 and ω_2, respectively. Vondràk (1985) used a similar procedure assuming, however, the annual frequency ω_1 to be constant. In sampling of $A_{CW}(\omega)$, there is a serious trade–off between the window length used to get one sample and the number of uncorrelated samples obtainable. To avoid a correlation between different samples, only non-overlapping windows should be used. If a small window length is selected, the number of samples increases, but the uncertainties for each of the samples increase as well, and if the window length becomes less than the beat period between CW and AW, the fit of eq. (27) becomes numerically instable. To assess the effect of the window length on the resonance parameters obtained from the fit of eq. (26) to $A_{CW}(\omega)$ window lengths from 6 to 25 years have been used and, in addition to eq. (27), also a base function of a harmonic circular rotation has been analyzed (see Fig. 1). Using this latter base function, both the prograde and retrograde CW have been investigated. Moreover, since

eq. (26) is non-linear in T_0 and Q, these parameters have to be determined iteratively, and the results may depend on the start values used. Therefore, a set of different start values have been used, too.

As expected from the discussion of the spectrum of the PM series given above, the retrograde wobble is highly variably in time and the pairs of instantaneous amplitudes and frequencies appear to be random for all window lengths. On the other hand, the prograde wobble clearly displays the amplitude-frequency relation shown in the previous section. Therefore, only the prograde wobble will be considered in the discussion below.

In Fig. 2 the instantaneous amplitudes and frequencies are exemplarily shown for a window length of 18 years. The respective resonance curves are displayed in Fig. 4 for both the X- and Y-components. The resonance periods and Q values obtained in these fits are roughly 450 days and 100, respectively. The period thus is considerably larger than those generally resulting in analyses of the total PM series (see Table 1). However, the largest periods are calculated for a window length of 18 years, while particularly for larger window lengths the periods are lower, thus tending to the value obtained from a fit of eq. (27) to the total PM series. There is no tendency for the X- and Y-components to produce systematically different values for T_0 or Q. In general, increasing the window length smoothes $A_{CW}(\omega)$, and the fit of the resonance curve results in a larger fraction of the variance of $A_{CW}(\omega)$ being explained. When small start values for Q are employed in the iterative fit of eq. (26) particularly for short window lengths, some fits may result in values for T_0 and Q scattering around 437 days and 30, respectively. However, these fits generally do not approximate the $A_{CW}(\omega)$ samples very well. Averaging over all window lengths and both PM components, the resulting resonance period and Q value are 444 ± 6 days and 85 ± 22, respectively.

A caveat is required here: the assumption of both, stationarity (i.e. a purely forced wobble) and constant amplitude of the quasi-periodic forcing may well bias the T_0- and Q-values given here. There is, however, no way of resolving this problem without knowledge of the excitation mechanism and the amplitude of the forcing.

The AW in PM is mainly attributed to atmospheric forcing (see e.g. Chao and Au, 1991). Therefore, we may use the resonance curve shown in Fig. 4 to derive the fraction of the annual forcing amplitude required to sustain a forced term in the Chandler band, too. In the spectrum, the CW amplitudes are not greater than 1.5 times the annual amplitude. At the annual frequency, the resonance curves determined by the different fits is between 5 and 10 % of the maximum at the resonance period. Thus, in the Chandler band, a forcing with an amplitude of 7.5 to 15 % of the annual forcing amplitude could suffice to maintain the observed wobble as a forced term.

Both, in ocean and atmosphere well-known signals exist in the Chandler band, which potentially are candidates for the quasi-periodic forcing mechanism. Therefore, in the next two section the relation of these signals to the CW and their capability to provide about 15 % of the annual forcing will be discussed.

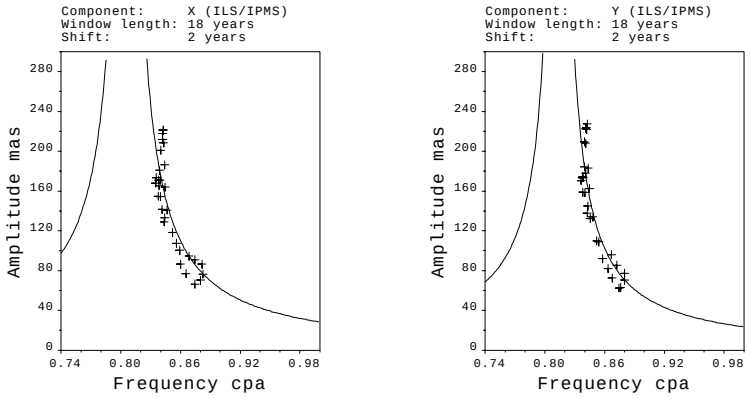

Fig. 4. Resonance curves for polar motion.

The resonance curves are shown for frequencies close to the maximum of the resonance. Crosses indicate the pairs of amplitude and frequency values determined in a least-squares fit of eq. (27) to the PM series. The resonance curves eq. (26) are fitted for an assumed "constant amplitude, variable frequency" forcing. The fit results in frequencies (periods) and Q values for the X and Y-components of $\omega_0 = 0.80586$ cpy ($T_0 = 453.2$ days), $Q = 77$ and $\omega_0 = 0.81400$ cpy ($T_0 = 448.7$ days), $Q = 104$, respectively. The resonance frequencies should indicate the "true" (and, of course fixed!) Chandler frequency if the "constant amplitude, variable frequency" assumption holds.

5 The pole tide

The most prominent oceanographic phenomenon in the CW band is, of course, the so-called pole tide, which is observed in nearly all coastal tide gauge records around the world. Shortly after the discovery of the CW, a fourteen-monthly signal was discovered in tide gauge recordings, too (Christie, 1900). This tide is commonly assumed to result from variations in the Earth's centrifugal potential due to the CW (see e.g. Munk and MacDonald, 1960). If this notion is realistic, then the pole tide would not be able to contribute to an excitation sustaining a forced CW.

As mentioned above, PM changes latitude and thus the centrifugal forces at a point. The potential Φ of the centrifugal force due to PM was given by Schweydar (1916) with

$$\Phi = -\frac{a^2\Omega^2}{2} \sin 2\theta (m_1 \cos\lambda + m_2 \sin\lambda), \tag{28}$$

where a is the Earth's radius, θ the co-latitude, and λ the (east) longitude. For a spherical Earth, the height ξ of the equilibrium pole tide in a global ocean is then

$$\xi(\theta,\lambda) = \frac{1 + k_2 - h_2}{g} \Phi(\theta,\lambda), \tag{29}$$

where g is the acceleration due to gravity, and k_2 and h_2 are the Love numbers for the changes in potential and the vertical displacement due to a body force of spherical degree 2. For a non-global ocean, mass has to be conserved. In a first order approximation, this can by achieved with the Darwin correction, which results in

$$\xi(\theta,\lambda) = -\frac{1+k_2-h_2}{g}\frac{a^2\Omega^2}{2}\cdot \left(\sin 2\theta(m_1\cos\lambda + m_2\sin\lambda) - \frac{m_1 a_2^1 + m_2 b_2^1}{5a_0^0}\right) \tag{30}$$

for the first order approximation of the equilibrium pole tide, where a_2^1, b_2^1 and a_0^0 are the coefficients of the spherical harmonic expansion of the ocean function (see e.g. Munk and MacDonald, 1960). For typical PM amplitudes of 200 mas, the pole tide amplitudes calculated from eq. (30) are of the order of 1 cm and lower.

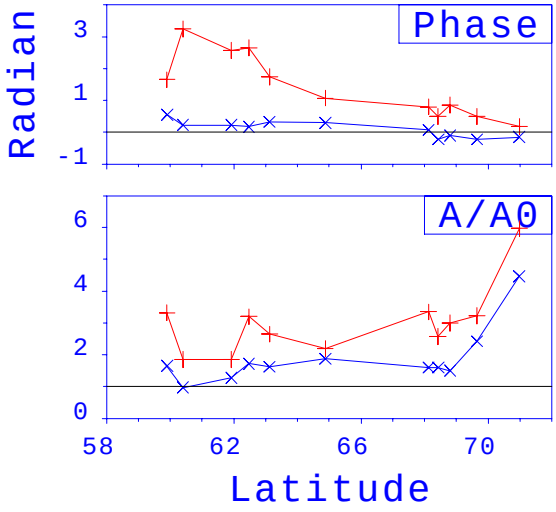

Fig. 5. Transfer function of the equilibrium pole tide.

The transfer function is given as an amplitude ratio and a phase difference between the observed signal and the equilibrium pole tide predicted from the observed PM. +: uncorrected monthly mean sea levels, x: after correction of the isostatic air pressure effect. From Plag (1988).

However, detailed studies of tide gauge records showed that in some regions the observed signal deviates from the equilibrium pole tide predicted from PM observations (Maksimov, 1954; Haubrich and Munk, 1959). In some regions like the Baltic Sea the deviation may reach more than ten times the equilibrium

amplitude and large phase shifts, and this has been a puzzling feature of the pole tide for the last 50 years. It has been taken as an indication for a dynamic answer of the ocean to PM forcing. The extent to which the pole tide is a dynamic tide determines the dissipation of the CW energy. Therefore, in the last twenty years, a number of theoretical studies and investigations of observations have attempted to solve this problem (see e.g. Dickman, 1979; Dickman and Steinberg, 1986; Dickman, 1988; Tsimplis *et al.*, 1994, and the references therein). Effects of a dynamical response of the ocean to PM forcing derived from hydrodynamical models for non-global oceans were found to be regionally of the order of 50 % of the equilibrium signal (Dickman, 1988) and thus is too small to explain the observed excess.

Naito (1977) was the first to show that globally the instantaneous period, amplitude and phase of the pole tide are temporally variable, but neither the period nor the amplitude of the pole tide are correlated with the instantaneous wobble parameters. Among others, Plag (1988) arrived at the same results; he showed that at the Norwegian coast most of the pole tide is due to an "inverse barometer" response of the sea level to an air pressure signal. His results are supported by Tsimplis *et al.* (1994), who used a meteorologically forced hydrodynamical tide and surge model of the North Sea to show that the non-equilibrium part of the pole tide in that region is fully accounted for by the meteorological forcing. In a recent study of the tide gauge data, Xie and Dickman (1996) arrived at similar conclusions. These results suggest that the atmosphere may contribute to PM excitation not only at the annual period but also in the CW band.

6 The fourteen-to-sixteen-months oscillation (FSO)

Maksimov (1954) and Maksimov *et al.* (1967) described a dominant air pressure signal with a period of about fourteen months which is most pronounced over the North Atlantic in the position of the Islandic low. Bryson and Starr (1977) and Starr (1983) discussed the relation between this meteorological signal and the CW and concluded that the atmospheric pole tide is not due to the CW. Plag (1988) studied the spatial distribution of the air pressure signal along the Norwegian Coast and found the amplitude increasing northwards, a feature contradicting the pattern expected for a CW induced pole tide. Furthermore, in this area, the amplitudes of the 14 months signal are nearly half the annual air pressure variations. He concluded that this atmospheric signal causes the excess of the observed sea-level signal with respect to the equilibrium pole tide at the Norwegian coast. More evidence for this signal in the atmosphere and the oceans to be of internal origin was produced from coupled atmosphere-ocean GCMs which exhibit eigenmodes at 14 months (Hameed and Currie, 1989; Currie and Hameed, 1990). However, the temporal variability of the observed fluctuations, i.e. their quasi-periodicity, is hardly explainable as being due to an eigenmode. The frequency of the signal in air pressure is temporally highly variable (Fig. 6), and these variations are correlated with those of the frequency of the apparent pole tide, while there is no simple correlation with the CW frequency. Thus, the

atmospheric signal cannot be explained as purely an atmospheric pole tide.

The period of the signals in sea level and atmospheric pressure is highly variable, which led Plag (1995) to denote the phenomena as the "Fourteen-to-Sixteen-months-Oscillation (FSO)". The high temporal and spatial correlation of the temporal variations in particularly the instantaneous periods underlines the coupled nature of the FSO in air pressure and sea level. Particularly in the North and Baltic Seas, the FSO masks the pole tide.

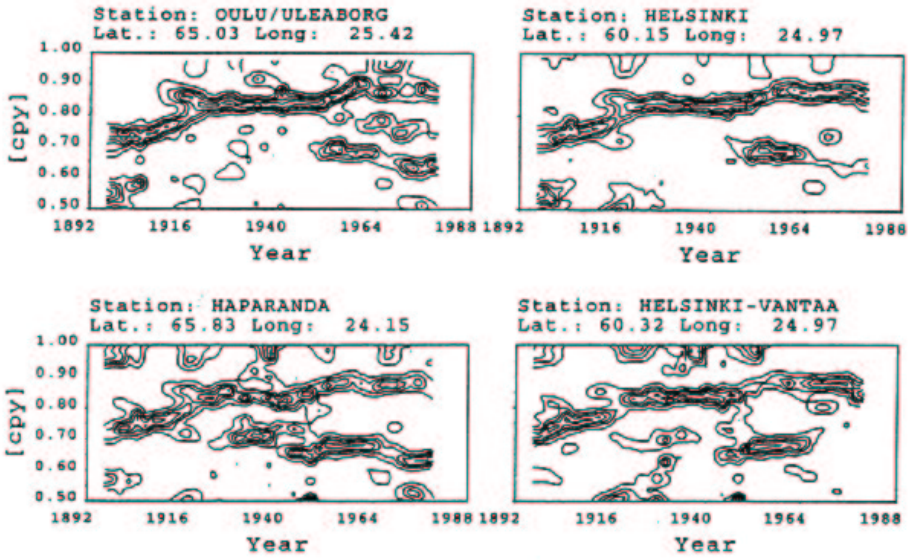

Fig. 6. FSO in sea level and air pressure.

Upper row: FSO in tide gauges; lower row: FSO in air pressure. The isolines are lines of constant variance, which are constructed from normalized variance spectra. For the spectra, a window length of 18 years is used. The base function includes an annual constituent to reduce the effect of this constituent on the interannual time scales.

It should be mentioned that in other meteorological and oceanic observations, a fourteen months signal has been detected, too. For example, Kikuchi and Naito (1982) describe variations of the sea-surface temperature in the Japan Sea.

Fig. 6 also shows that the frequencies do not vary uniformly in time. There are several intervals, where the FSO displays a nearly constant frequency, and these long stable intervals are interrupted by short intervals of rapid to jump-like variations in the frequency. Based on the oceanic FSO, where this pattern is slightly more pronounced, four steps can be identified within the last 90 years (Table 2). Applying this segmentation of the FSO to the northern hemispheric mean temperature record, significant jumps in the mean temperature of the different segments are found (Fig. 7) which break the general temperature increase

Table 2. Time intervals with stable periods of the FSO.

The periods given are mean values determined for the oceanic FSO all suitable tide gauge records in the North and Baltic Seas. The period before the jump around 1902 could not be determined due to lack of data. From Plag (1993).

Interval	Mean Period days	Jump days
1903-1919	480±1	
1920-1955	436±1	-44 ± 1
1956-1978	418±1	-18 ± 1
1979-1991	430	12

over the last 100 years into a sequence of a few distinct jumps. No such segmentation is found for the southern hemisphere, where the mean temperature displays a nearly linear increase.

Some of the jumps in the northern hemispheric temperature are well known among climatologists (particularly the one around 1920, see Ellsaesser *et al.*, 1986, for more references). Thus, jumps in the frequency of the FSO seem to correlate with jumps in hemispheric temperature. On the other hand, Schlesinger and Ramankutty (1994) describe an oscillation of 65-70 years in the (smoothed) mean temperature of the northern hemisphere, which is most pronounced over the North Atlantic (Fig. 8). This oscillation is in agreement with the strongly smoothed jump sequence, and thus it is not clear whether there is a more or less harmonic variation in the hemispheric temperature or rather an indication of rapid transitions between different states of the hemispheric climate system. It is clear, that unraveling this problem is of particular weight for understanding climate variability on interannual to interdecadal time scales, and these time scales are of paramount interest for predicting future anthropogenic climate variations.

The restriction of the phenomenon (i.e. the oscillation of 65-70 years and the segmentation determined from the FSO) to the northern hemisphere may indicate an influence of the land-ocean distribution, which is markedly different on the two hemispheres.

7 Model predictions of polar motion due to atmospheric excitation

Returning to the question of what is forcing the observed CW, a combination of the FSO and the oscillation of 65-70 years described in the previous section will be used to construct an atmospheric forcing function for the ELE given in section 2. Eqs. (18) are set up for an Earth model with a viscoelastic mantle and fluid core, and the excitation functions given by eq. (20) include a first order approximation of an equilibrium ocean. To predict PM due to a given forcing, these equations are integrated over time. However, modeling atmospherically forced PM over time intervals of 10^2 years introduces several problems. The

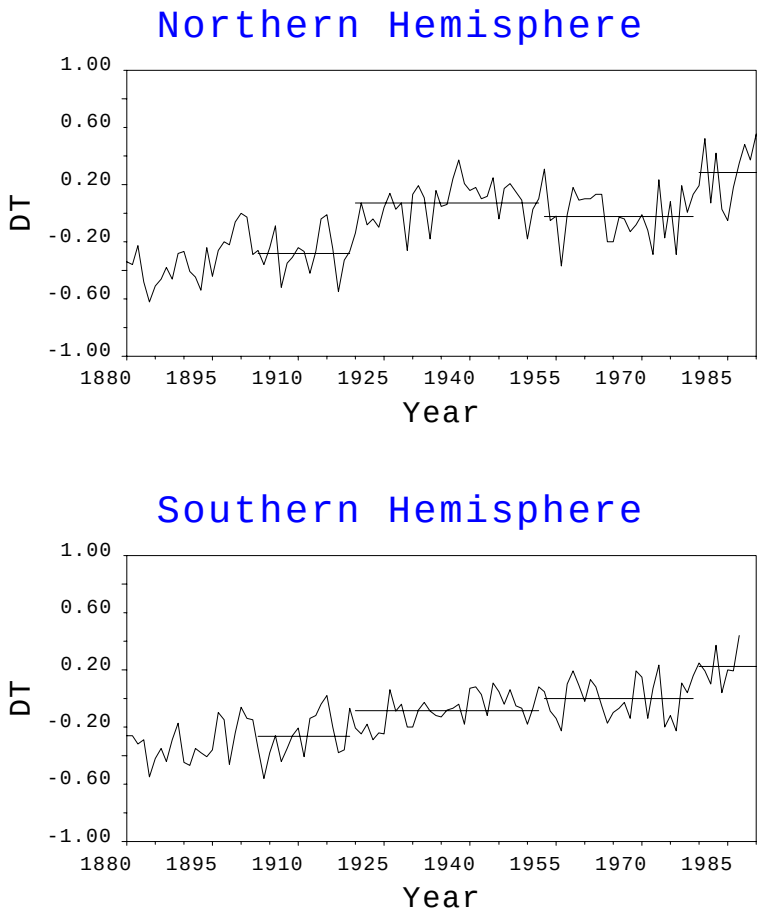

Fig. 7. Segmentation of hemispheric temperature anomalies.

DT denotes temperature anomalies (in K), which are taken from Jones *et al.* (1986)) and Jones (1992, personal communication). The horizontal lines indicate the mean value of the temperature anomalies within the segments defined by the frequency jumps of the FSO. Note that for the northern hemisphere the temperature steps around 1920 and 1978 are as large as 0.35 K.

atmospheric and oceanic data base available for the last hundred to two hundred years is not sufficient to be used directly as input for the PM equations. The observational evidence therefore needs to be interpolated somehow. The initial conditions excite a free damped CW, which requires a long time before being sufficiently damped. Thus, a considerable time interval is needed to reduce the effect of the initial conditions in the predicted PM series. Therefore, the forcing

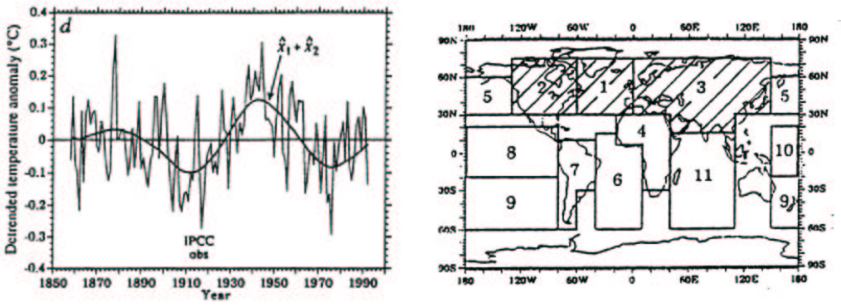

Fig. 8. The 65-70 years oscillation in temperature.

Left: temporal variation of the oscillation of 65-70 years in the mean temperature of the northern hemisphere ($\hat{x}_1 + \hat{x}_2$). Right: geographical regions, in which the oscillation is most pronounced (hatched areas). According to Schlesinger and Ramankutty (1994).

function needs to be extended before the time interval actually being of interest, i.e. back into the last century.

The coupled atmosphere-ocean FSO loads and deforms the solid Earth and thus, in principle, is capable of forcing PM. Particularly when the instantaneous frequency of the FSO is close to the (still unknown) eigenfrequency of the Earth in the Chandler band, the effect of the FSO on PM would be strong. Therefore, the temporal variations of the FSO frequency may be crucial for PM excitation. The spatial distribution of the FSO in both sea level and air pressure is in agreement with the spatial extent of the oscillation of 65-70 years as given by Schlesinger and Ramankutty (1994). Therefore, the atmospheric forcing function includes a FSO in air pressure with a spatial extent as given in Fig. 8. In addition, an annual forcing term is included in order to determine the amplitude ratio of the predicted AW and CW. Before 1902, when the first detectable frequency shift in the FSO occurred, the excitation consists of a annual constituent and a fixed-frequency FSO.

The PM series predicted for this forcing function (Fig. 9) are analyzed in the same way as the PM observations. The resulting instantaneous amplitudes and frequencies of CW and AW shown in Fig. 10 are similar to those of the observed wobbles (Fig. 2). Moreover, a variety of different forcing functions with and without the FSO were used as input for the model equations, proving that only those including the FSO in the way described above predict a CW with characteristics similar to those of the observed CW. In this case, a FSO in air pressure with an amplitude of only 50 Pa is sufficient to excite the CW with amplitudes of the same order as the observed ones.

The resonance curves fitted to the pairs of instantaneous amplitudes and frequencies result in values for T_0 and Q of the predicted CW of 437.6 days and 230. It is interesting to note that the free mode period built into the model is

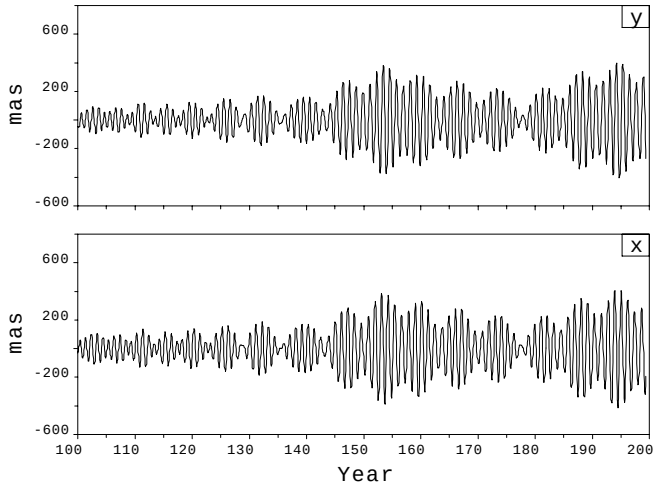

Fig. 9. Predicted polar motion due to atmospheric forcing.

Time in years after the start of integration. The excitation is consistent with a start of integration at 1800. The atmospheric excitation includes an annual constituent and a FSO with spatial extent given by the hatched area in Fig. 8 and temporal variations of the period as given in Table 2.

435.0 days, thus, the period determined in the analysis of the predicted PM is slightly longer than the actual free period. The free mode in the model has a damping of 100 whereas the analysis of the predicted forced wobble damping of the model leads to a Q 15 —5 larger than that. This may be taken as an indication that the T_0 and Q determined for the observed CW are also tending to be slightly larger than the respective parameters of the free wobble of the real Earth.

8 Conclusions

The characteristics of the observed CW are in agreement with those expected for a resonant forced oscillation. Therefore, the hypothesis forwarded here to explain the features of the CW derived from PM observations considers the wobble to be mainly a forced motion instead of a purely free one. Under this hypothesis, the resonance frequency (i.e. the "true" Chandler frequency) is fixed in time, while the forcing frequency is variable, thus producing the characteristics of a resonance curve in the observed CW. Fitting a resonance curve to the instantaneous parameters of the observed CW, the resonance period turns out

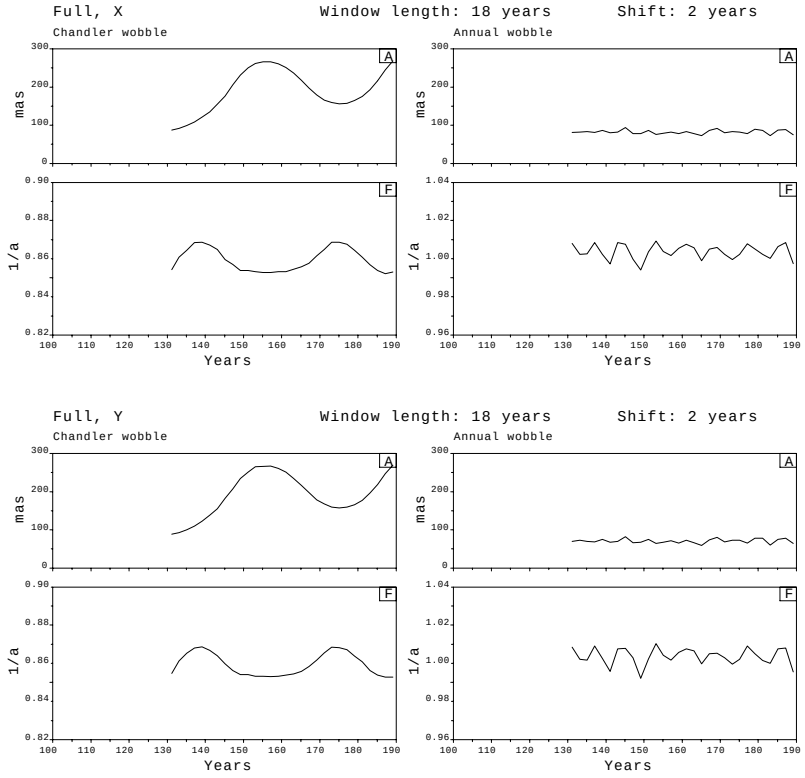

Fig. 10. Instantaneous amplitudes and frequencies of predicted annual and Chandler wobbles.

For an explanation see Fig. 2.

to be significantly larger than the widely accepted approximately 435 days. In a recent study, Kuehne *et al.* (1996) arrive at a similar conclusion finding the free wobble period to be 439.5 days. In study of this type, excitation functions are derived in a demodulation of the PM observations and are correlated with other observations such as AAM series. In Kuehne *et al.* (1996) the determination of the period is based on a least squares fit of excitations functions derived from 9 years of recent PM observations combined with proxy excitations constructed from atmospheric data. The fit is then backed by extensive Monte Carlo tests. The result obtained by Kuehne *et al.* (1996) appears to be in contrast to that of Furuya and Chao (1996), who base their study on 10.8 years of modern PM observations together with AAM data. Proceeding in essentially the same way as Kuehne *et al.* (1996) but making fuller use of the AAM observations, the Monte Carlo test leads them to a best estimate of the CW period of 433.7 days.

If, however, the observed CW has a strong forced part, as was demonstrated in the previous sections to be in agreement with the characteristics of the observed PM, with the forcing not fully represented by the atmospheric or proxy data, then the methodology applied by Kuehne *et al.* (1996) and Furuya and Chao (1996) can be expected to result in different (apparent) CW periods for different time intervals.

The forcing mechanism in the Chandler band may well be the FSO, which is a quasi-periodic oscillation of the coupled atmosphere-ocean system. In all studies of CW excitation, the possible role of the ocean has been neglected, due to insufficient amount of observations. If, as the pieces of evidence discussed here do suggest, the oceans significantly take part in this FSO, the missing contribution for sustaining the observed wobble may stem from the combined effect of the atmosphere and oceans.

Furuya and Chao (1996) refer to a study by Furuya *et al.* (1996), where quasi-periodic wind signals in the Chandler band are considered as possible excitation of the CW. However, these wind signals are likely to be correlated with the FSO in pressure (see Plag, 1988) and thus may not rule out the pressure forcing as the major forcing of PM in the Chandler band. In fact, as reported in the previous section, in model studies the pressure forcing due to the FSO is found to be sufficient to excite the PM in the Chandler band. Moreover, Volland (1996) rules out wind as a major forcing factor for PM and concludes that only atmospheric pressure loading contributes to atmospheric PM excitation. He finds Rossby-Haurwitz waves in the atmosphere with amplitudes of the order of 50 Pa to be sufficient to excite the PM in the Chandler band. Interestingly, such waves can be excited by suitably heating the atmosphere from below (Volland, 1994, personal communication). Ideally, such heating would have a sectorial spatial pattern. Thus, if the FSO is such a Rossby-Haurwitz wave, its restriction to the northern hemisphere alone could be a consequence of the hemispheric differences in the land-ocean distributions, which are nearly sectorial and zonal in the northern and southern hemispheres, respectively.

However, if this turns out to be right, this does not answer the question concerning the ultimate cause, since the origin of the FSO in the atmosphere has not been discussed yet. To understand this signal, the complete interannual meteorological spectrum has to be considered, which exhibits a number of additional quasi-periodic fluctuations such as the quasi-biennial oscillation. Plag (1988) suggested a non-linear response of the atmosphere to the solar forcing as a possible mechanism creating most of the observed interannual signals. The slight modulation of the annual cycle in insolation due to the quasi-periodic solar sunspot cycle, in principle, has the potential of creating a large set of interannual frequencies, with these frequencies coinciding with most of those frequently reported in the interannual part of meteorological or oceanographic spectra. In the non-linear atmosphere-ocean system, the amplitudes of the system's response to these modulation frequencies may be considerable, and ultimately, we may find that they contribute substantially to the interannual spectrum of the atmosphere-ocean system.

As discussed in the previous section, a FSO with amplitude of only 50 Pa is sufficient to excite the PM in the Chandler band. This high sensitivity of the PM to atmospheric forcing requires atmospheric data of high quality as input for polar motion models. However, vanDam *et al.* (1994) pointed out that, for example, the global atmospheric data set of the National Meteorological Centers (NMC) only poorly represent air pressure at high latitudes with differences between the global data set and station data of up to 3000 Pa. Unfortunately, the FSO has large amplitudes particularly at high latitudes. Therefore, it cannot be expected that the atmospheric excitation of the CW can be modeled on the basis of these data.

The high sensitivity of the CW could, however, be used in the validation process of climate models. Using the air pressure field predicted by climate models for the last 100 years as input for a (sufficiently complex) polar motion model, the predicted PM should exhibit a CW with characteristics comparable to those of the observed wobble. If not, the climate models would not be accounting for the FSO, which may turn out to be a major feature of the atmospheric circulation over the northern hemisphere.

A Properties of the polar motion data

Most recent papers concerning the interannual part of the spectrum of (PM) are based upon the 80 years record derived from the combined observations of the International Latitude Service (ILS) and the International Polar Motion Service (IPMS). This series starts in 1900 and is derived from optical astrometric observations at a varying number of stations (Yumi and Yokoyama, 1980). A second frequently used but somewhat shorter record starts in 1964 and was, until 1988, supplied by the Bureau International de l'Heure (BIH). Currently, the data set is updated by the International Earth Rotation Service (IERS). This latter record results from a number of different observation techniques such as Satellite Laser Ranging, Lunar Laser Ranging and Very Long Base Line Interferometry (Kolaczek, 1989).

Though the Earth rotation parameters (ERP) based on space techniques have a precision about an order of magnitude better than those determined from astrometric methods, the long astrometric series will continue to be important for quite a long time to come. They constitute a unique source of our knowledge of the past PM. On time scales from months to years there are, however, systematic differences between the astrometric PM and those determined from VLBI and SLR, and these differences are still not completely understood (e.g. Kolaczek and Hua, 1991).

For our study of the nature of the 14-monthly oscillation in PM, commonly termed the CW, the temporal variability is an important criterion. Therefore, both the length of the series as well as the data homogeneity are important in selecting the data, and the results are heavily dependent on the quality of the PM data used. Therefore, we will first assess the long series to decide which of these is best suited for studies of long-term characteristics of the CW. Besides

the ILS/IPMS series mentioned above, there are two more long PM series (see Tab. 3), one of them being a reanalysis of the ILS/IPMS data performed by Gross (1990), the other one being compiled and distributed by the IERS. This latter series is a combination of PM data obtained by different methods of observation covering the period from 1854 to 1993.

Table 3. Available PM series.

Series given in the lower part of the table are too short to derive the temporal variability of the observed CW.

Abbreviation and Source	Interval	Sampling interval
ILS/IPMS, Yumi and Yokoyama (1980)	1899 - 1979	1 month
GROSS, Gross (1990)	1899 - 1979	1 month
IERS93 (C04)	1845 - 1993	1 month
BIH	1969 - 1985	5 days
VLBI	1981 - 1992	1 to 5 days
IERS/ERP (C01)	1963 - 1993	1 day

The origin of the ILS/IPMS astrometric observations has been reviewed by e.g. Lambeck (1980), who also gives an account of possible sources of data inhomogeneities and errors. In a great effort, Yumi and Yokoyama (1980), denoted by YY) used the original observations to derive the homogeneous series of the ILS/IPMS PM data for the period 1899.0 to 1979.0. In YY, the observed latitude variations $\Delta\phi_i$, where i denotes the station number, are fitted by

$$\Delta\phi_i = x(t)\cos\lambda_i + y(t)\sin\lambda_i + z(t), \tag{31}$$

where ϕ_i and λ_i are the geographical latitude and longitude, respectively, of the $i-$th station. $x(t)$ and $y(t)$ are the displacements of the pole towards 0° and 90° W, respectively, relative to an arbitrary origin. $z(t)$ is a station-independent error term introduced by Kimura to increase the overall quality of the fit (see e.g. Lambeck, 1980). The resulting series are given as monthly values of the x- and y-coordinates of the pole position and the Kimura error term. These PM series stimulated a number of analyses (e.g. Dickman, 1981; Daillet, 1981; Chao, 1983; Guinot, 1982), but the analyses did not succeed in clarifying the open questions concerning the properties of the CW.

Vondràk (1985) used a data set comprising the ILS/IPMS data augmented by the more recent BIH and some additional data. His series were not available for the present study, but some of his results will be discussed further below.

Gross (1990) reanalyzed the original ILS/IPMS data to obtain new PM series. The difference between YY's analysis and the Gross analysis lies in the treatment of the error term, i.e. the Kimura term. Gross assumes a station-dependent error and uses

$$\Delta\phi_i = x(t)\cos\lambda_i + y(t)\sin\lambda_i + z_i(t), \tag{32}$$

instead of (31) to fit the observations. In the Gross-analysis, the system of normal equations is underdetermined, requiring additional constraints (see Gross, 1990, for more details).

The longest PM series covering the interval from 1854 to 1992 are supplied by the IERS. However, these series are a conglomerate of different data sets originating from different observational methods (see below).

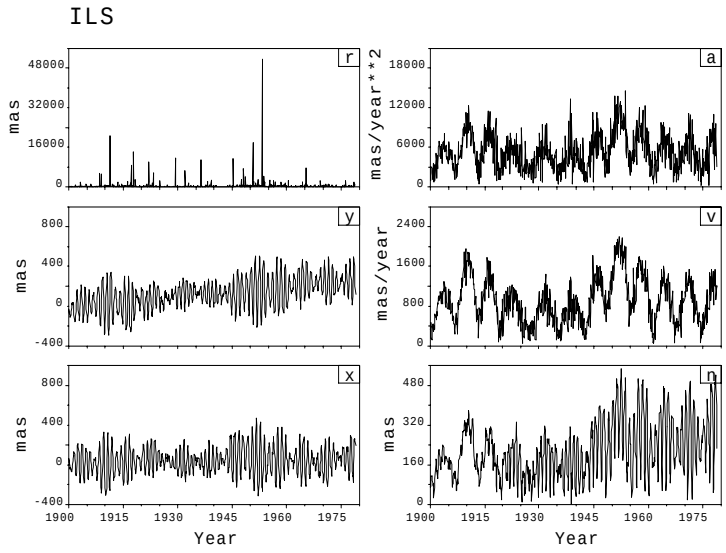

Fig. 11. Characteristics of the ILS/IPMS polar motion series.

The pole position is considered as a path in $\mathbb{R}^2$. The diagrams x and y are the $X-$ and $Y-$coordinates of the pole position in milliarc seconds, respectively, n is the norm, v the velocity, a the acceleration and r the radius determined as described in the text.

To assess the data homogeneity, the pole path is considered as a function in $\mathbb{R}^2$, i.e.

$$\mathbf{s}(t) = \begin{pmatrix} x(t) \\ y(t) \end{pmatrix}. \tag{33}$$

From this function, a number of parameter functions are derived, which will be used for the assessment the data quality. Thus norm

$$n(t) = \|\mathbf{s}(t)\| = \sqrt{x^2(t) + y^2(t)}, \tag{34}$$

the velocity

$$v(t) = \left\| \frac{d\mathbf{s}(t)}{dt} \right\| = \sqrt{\left(\frac{dx(t)}{dt}\right)^2 + \left(\frac{dy(t)}{dt}\right)^2}, \tag{35}$$

and the acceleration

$$a(t) = \left\| \frac{d^2\mathbf{s}(t)}{dt^2} \right\| = \sqrt{\left(\frac{d^2x(t)}{dt^2}\right)^2 + \left(\frac{d^2y(t)}{dt^2}\right)^2}, \tag{36}$$

are calculated for all series.

The curvature κ of the path could be calculated from

$$\kappa(t) = \frac{\|\mathbf{v}(t) \times \mathbf{a}(t)\|}{v^3(t)} , \tag{37}$$

but this formula is inconvenient for numerical calculations and somewhat inaccurate due to the numerical differentiations involved. Therefore, alternatively, the calculation of the radius of curvature

$$r = \kappa^{-1} \tag{38}$$

by fitting a circle to three consecutive pole positions is preferred. All these parameters help to discuss some of the properties inherent in the PM, which are of potential importance in understanding the CW.

Starting with the ILS/IPMS series, Fig. 11 displays the x- and y-coordinates of the pole position together with the parameters derived from the pole path. In the coordinate system used by the ILS/IPMS to represent the pole position the x-axis points toward the longitude $\lambda = 0°$ (Greenwich) while the y-axis points to $\lambda = 90°$ W. In both, the x- and y-coordinate of the pole position, the characteristic beat due to the superposition of AW and CW is the most prominent feature. This superposition also produces the protruding variation of about 5 to 8 years duration in both velocity and acceleration.

Especially the norm and the velocity show that the whole record separates into three distinct parts: Between 1900 and about 1920, the beat of CW and AW is characterized by a period of about 6.5 years and a comparatively large amplitude. Within the second part from 1920 to about 1943, the beat amplitude is rather small while the period is almost 8 years. The third part again is characterized by a larger beat amplitude and a smaller beat period.

Leaving Fig. 11 for a moment, the other two long series will be considered. In Fig. 12 the characteristics of the reanalysis of the ILS/IPMS data by Gross (1990) are shown. As was discussed above, the basic difference between the YY-analysis and the Gross-analysis lies in the treatment of the error term (see equations 31 and 32). A high frequency noise is present in the Gross-series, as is most obvious in the acceleration, while the overall characteristics of the pole path are more or less the same for both analyses. There are also some pronounced differences, which are most obvious in the interval 1925–1930 and around 1973, where the characteristic pole path due to CW and AW is almost below the noise level. In the norm of the Gross series, the CW and AW appear right from the start, which implies an origin different from that of the ILS/IPMS series. In the norm, some pairs of adjacent maxima have exchanged their ranks compared to the YY-series (e.g. around 1955 and 1976). The higher noise level of the Gross series might well be due to numerical problems in the solution of the normal equations of the fit of (32) to the observations. Therefore, the original YY series seem to be better representing the actual PM.

At a first glance, the IERS monthly series covering the interval from 1854 to 1993 is most attractive due to its length of almost 150 years. However, Fig. 13

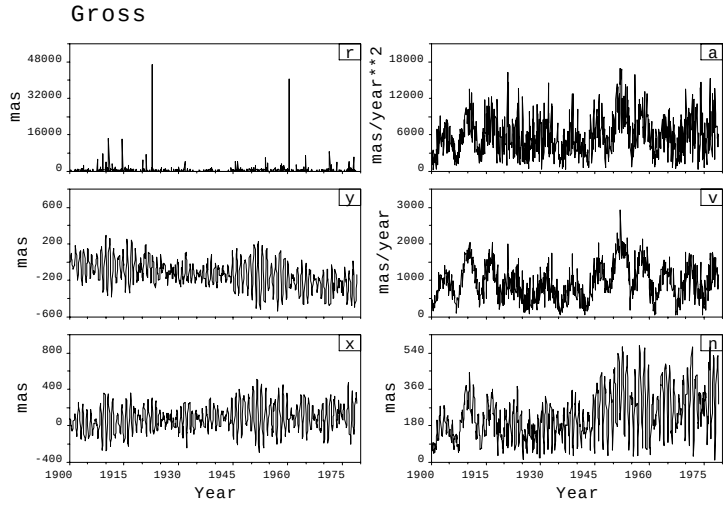

Fig. 12. Characteristics of the Gross polar motion series.

See Fig. 11 for an explanation. Note that Gross (1990) used a coordinate system with the y-axis pointing towards the 90° E meridian instead of the 90° W as used by the other series. The Gross-series have a higher noise level compared to the YY solution (see text), as is best illustrated by the acceleration and the radius.

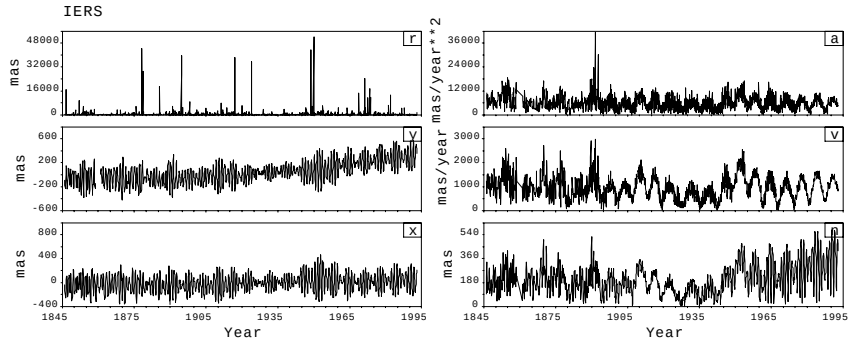

Fig. 13. Characteristics of the IERS monthly polar motion series.

See Fig. 11 for an explanation. Note the sudden changes in the characteristics of particularly the acceleration and the radius at about 1895. These changes are taken as evidence for data inhomogenieties. For r the same scale as in Fig. 11 is used, though the maximum values are as large as 10^6 mas.

reveals severe data inhomogeneities, with the complete record separating into at least three distinct parts. The first part prior to 1895 is characterized by a high noise level and large kinks indicated by very large values of the acceleration and the radius (up to 10^6 mas). The part between 1900 and 1979 is more or less comparable to the YY-series, though there are still some discernible differences. After 1979, the noise in velocity and acceleration decreases strongly, which is characteristical for the strongly filtered BIH data (see e.g. Guinot, 1978).

Due to these inhomogeneities, the IERS series are virtually useless for any long-term studies. It should even be stressed here, that using such inhomogeneous data might result in the detection of apparent phenomena being solely due to artificial effects. As will be discussed elsewhere, the same characteristics described here for the IERS monthly series are found for the IERS daily data (see Tab. 3) supplied for the interval from 1962 to 1993. Here, too, the most protruding properties of the data are the inhomogeneities!

In what follows, this study will be based on the series resulting from the original YY-analysis. Returning to Fig. 11, the norm reveals another interesting fact: during the first part of the record, the motion is mainly about the center of coordinates, and the CW and AW do not appear in the norm. Around 1920, the wobbles appear in the norm, and another change of the norm is discernible around 1943. During each intermediate part, the pattern of the norm is seemingly stable. The feature may be due to both, an increase in the amplitudes of the wobbles and a more or less sudden shift of the center of motion. The latter of these causes introduces a step function rather than a linear trend in the instantaneous center of motion, and this might result in a serious bias of the results of any temporal analysis. Therefore, it is worthwhile trying to exclude the latter cause as being responsible for the changes in the norm. For this purpose, statistical tests for sudden changes within time series may be utilized. The Mann-Kendall-Sneyers sequential test resulting in the so-called C-functions is one of those tests (see e.g. Sneyers, 1975; Kendall and Stuard, 1979), and has been successfully applied to different geophysical time series by e.g. Goossens and Berger (1986, 1987) and Demaree and Nicolis (1990). For the data points $x_1, ..., x_n$ this non-parametric test is based on Mann's rank statistics, which gives, for each sample x_i, the number n_i of preceding samples x_j $(j < i)$, with $x_j < x_i$. Under the null hypothesis (i.e. stationary data, no trend), the test statistics

$$t_k = \sum_{i=1}^{k} n_i \tag{39}$$

is normal distributed and the mean and variance of t_k are given by

$$\overline{t_k} = \frac{k(k-1)}{4} \tag{40}$$

and

$$\overline{\delta t_k^2} = \frac{k(k-1)(2k+5)}{72}, \tag{41}$$

respectively. For the normalized variable

$$u_k = \frac{t_k - \overline{t_k}}{\sqrt{\overline{\delta t_k^2}}} \tag{42}$$

the probability

$$\alpha = \text{prob}(|u_\alpha| < |u_k|) \tag{43}$$

is used to accept or reject the null hypothesis. For any significance level α_0 of the test, a corresponding level of u_0 can be determined. For $\alpha_0 = 0.05$, the corresponding value of u_0 is 2.03 (Goossens and Berger, 1986). In the sequential version of this test, both forward and backward functions of u_k are calculated (the so-called C-functions), and an intersection of the two function within the confidence interval may be used to determine the time of the onset of either a trend or a rapid change like a step. The C-functions of the detrended x- and y-coordinates of PM (Fig. 14) do not indicate a step where the characteristics of the norm and velocity change. Therefore, it may savely be concluded that these changes are merely due to an increase in the CW amplitude.

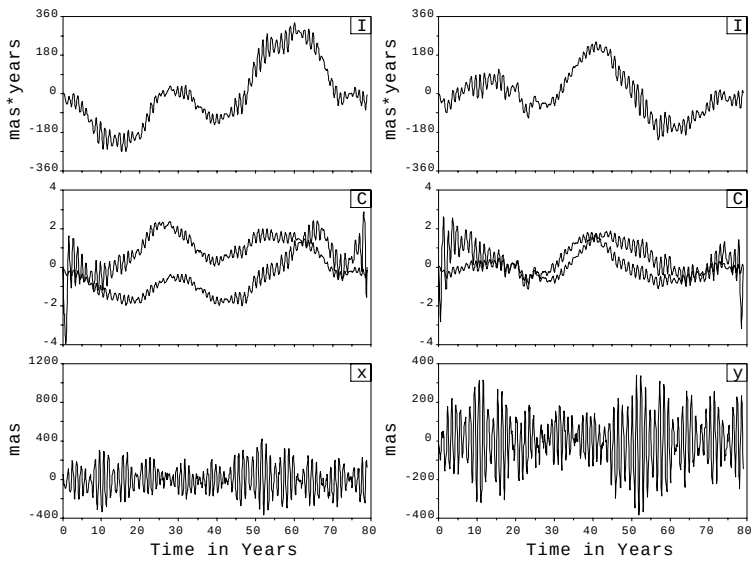

Fig. 14. C-functions of the polar motion components.

The lower diagrams display the detrended x- and y-coordinates of the pole position. In the middle diagrams, the C-functions are given for the two coordinates separately. The C-functions are calculated for the detrended data according to Goossens and Berger (1986). Confidence limits for 95 % are at ± 2.03. The upper diagrams show the integrals of the two detrended components.

In Fig. 14, the integrals $I_x(t) = \int_0^t x(s)ds$ and $I_y(t) = \int_0^t y(s)ds$ of the detrended coordinates are plotted. The integral is a rather effective low pass filter. An interdecadal fluctuation clearly emerges from both components, which has been termed as Markowitz wobble (e.g. Dickman, 1981; Vondràk, 1985). Denoting this fluctuation a wobble is still a matter of discussion, and this topic will be taken up again elsewhere.

It is of interest to compare the long time series to the more precise series based on space-geodetic techniques. Therefore, one of the three shorter data sets mentioned in Tab. 3 will be considered, namely the ERP series available from the BIH. The unsmoothed BIH PM-series exhibit features in x, y, and the norm, which are similar to those of the YY series (Fig. 15). The norm indicates that the center of motion is not identical to the origin. Both, velocity and acceleration display large variations in the beginning, which could well be due to larger uncertainties in the measurements. For the velocity, the characteristic beat emerges somewhere after 1970, while for the acceleration no such feature is discernible. Furthermore, the scale for the BIH acceleration is larger than for the ILS acceleration by more than one order of magnitude. This increase in acceleration is most likely due to the shorter sampling interval, which is five days for BIH compared to one month for ILS.

Comparing directly the pole paths as given by the ILS/IPMS series and BIH series (Fig. 16), the stronger short period noise in the unsmoothed BIH data is obvious, while the long-term pattern is the same for both data sets. There are, however, some protruding differences between the ILS/IPMS and the BIH data, that are not explainable by the high-frequency noise level in the BIH data. These differences indicate the level of uncertainty in the individual ILS/IPMS values, which are higher than the uncertainties ascribed to the individual observations. The source of these systematic differences investigated in more detail by Kolaczek and Hua (1991) remains unknown.

The radius of curvature has not yet been considered. Taking into account the different features for the acceleration, the similarity of this parameter calculated from the different data sets including the BIH data is rather striking. For most of the time, the radius is varying rather smoothly between 100 and 300 mas. However, frequently there are large spikes, amounting to seconds of arc and occasionally radii of as much as 35,000 mas and 90,000 mas may occur for the ILS/IPMS and BIH data, respectively. It is interesting to note that of all available series, the YY data not only exhibit the smoothest acceleration but also the least spikes in the radius. These spikes fix the points of departure from a smooth polar path, and they are related to the kinks already noted by Mansinha and Smylie (1970). They also found a correlation between these kinks and the occurrence of large earthquakes, but these results were questioned on both, observational (Haubrich, 1970) and theoretical basis (Dahlen, 1971, 1973). Recently, Preisig (1992), making use of high precision PM data, again related irregularities of the polar path to large earthquakes. Eventually both, acceleration and radius of the polar path may be used for the search of correlations between geodynamic events and PM. Especially in high precision data such as the IRIS data, these

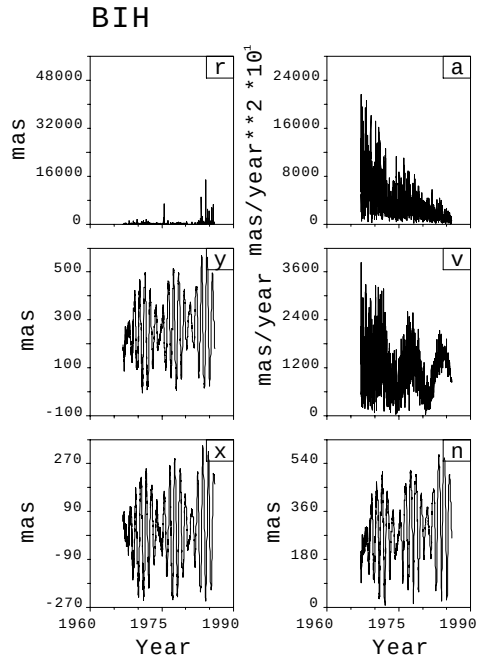

Fig. 15. Characteristics of the BIH polar motion data.

See Fig. 11 for explanation. Data are the unfiltered BIH series. Note the different scales for the acceleration in the present figure compared to Fig. 11, which may be due to the shorter sampling interval for the BIH series (see Tab. 3). The decrease of the high frequency-noise in both, velocity and acceleration is an indicator of the data quality increasing with time.

parameters may potentially be of importance, but they will not be discussed here any further.

Summarizing the discussion of the available long series of PM, it is concluded that the ILS/IPMS series are best suited for studying the long-term variability of the CW. Comparing the ILS/IPMS data to the BIH data indicates the individual values to carry uncertainties, which sometimes may be quite large. However, the long-term stability of the series seems to be sufficient enough to study the temporal variability of the CW.

Acknowledgements

The PM data was supplied by the ILS in Mizusawa, the former BIH, Richard Gross and the IERS. The author would like to thank these institutions and per-

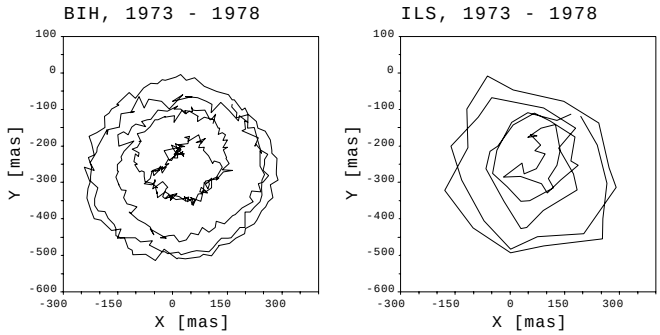

Fig. 16. Comparison of the ILS/IPMS and BIH pole paths.

The data have been converted such that the positive y-axis points towards the 90° E meridian.

sons. Also appreciated are the many discussions with V. Rautenberg, J. Zschau, H.-U. Jüttner and P. Ruf, who carefully read the manuscript and made numerous helpful comments.

References

Barnes, R. T. H., Hide, R., White, A. A., and Wilson, C. A. (1983). Atmospheric angular momentum fluctuation, length-of-day changes and polar motion. *Proc. Royal Soc.*, **A 387**, 31–73.

Bryson, R. A. and Starr, T. B. (1977). Chandler tides in the atmosphere. *J. Atmos. Sci.*, **34**, 1975–1986.

Carter, W. E. (1981). Frequency modulation of the Chandlerian component of polar motion. *J. Geophys. Res.*, **86(B3)**, 1653–1658.

Chandler, S. C. (1891). On the variation of latitude, II. *Astron. Jour.*, **XI (9)**, 65–70.

Chandler, S. C. (1892). On the variation of latitude, VII. *Astron. Jour.*, **XII (13)**, 97–101.

Chandler, S. C. (1893). On the variation of latitude, VIII. *Astron. Jour.*, **XIII (19)**, 159–162.

Chandler, S. C. (1902). . *Astron. Jour.*, **22**, 154.

Chao, B. F. (1983). Autoregressive harmonic analysis of the Earth's polar motion using homogeneous International Latitude Service data. *J. Geophys. Res.*, **88(B12)**, 10299–10307.

Chao, B. F. and Au, A. Y. (1991). Atmospheric excitation of the earth's annual wobble: 1980-1988. *J. Geophys. Res.*, **96**(B4), 6577–6582.

Christie, A. S. (1900). The latitude variation tide. *Bull. Phil. Soc. Washington*, **13**, 103–122.

Colombo, G. and Shapiro, I. I. (1968). Theoretical model for the Chandler wobble. *Nature*, **217**, 156–157.

Currie, R. G. and Hameed, S. (1990). Atmospheric signals at high latitudes in a coupled ocean-atmosphere general circulation model. *Geophys. Res. Lett.*, **17**, 945–948.

Currie, Robert G. (1974). Period and Q_w of the Chandler Wobble. *Geophys. J. R. astr. Soc.*, **38**, 179–185.

Dahlen, F. A. (1971). The excitation of the Chandler wobble by earthquakes. *Geophys. J. R. astr. Soc.*, **25**, 157–206.

Dahlen, F. A. (1973). A correction to the excitation of the Chandler wobble by earthquakes. *Geophys. J. R. astr. Soc.*, **32**, 203–217.

Daillet, S. (1981). Secular variation of the pole tide: correlation with Chandler Wobble ellipticity. *Geophys. J. R. astr. Soc.*, **65**, 407–421.

Demaree, G. R. and Nicolis, C. (1990). Onset of Sahelian drought viewed as a fluctuation-induced transition. *Q. J. R. Meteorol. Soc.*, **116**, 221–238.

Dickman, S. R. (1979). Continental drift and true polar wandering. *Geophys. J. R. astr. Soc.*, **57**, 41–50.

Dickman, S. R. (1981). Investigation Of Controversial Polar Motion Features Using Homogeneous International Latitude Service Data. *J. Geophys. Res.*, **86(B6)**, 4904–4912.

Dickman, S. R. (1988). The self-consistent dynamic pole tide in non-global oceans. *Geophys. J. Int.*, **94**, 519–543.

Dickman, S. R. and Steinberg, J. R. (1986). New aspects of the equilibrium pole tide. *Geophys. J. R. astr. Soc.*, **86**, 515–529.

Ellsaesser, H. W., MacCracken, M. C., Walton, J. J., and Grotch, S. L. (1986). Global climatic trends as revealed by the recorded data. *Rev. Geophys.*, **24(4)**, 745–792.

Furuya, M. and Chao, B. F. (1996). Estimation of period and q of the Chandler wobble. *Geophys. J. Int.*, **127**, 693–702.

Furuya, M., Hamano, Y., and Naito, I. (1996). Quasi-periodic wind signal as possible excitation of Chandler wobble. *J. Geophys. Res.* in press.

Gaposchkin, E. M. (1972). Analysis of pole positions from 1846–1970. In P. Melchior and S. Yumi, editors, *Rotation of the Earth*, pages 19–32. D. Reidel, Dordrecht.

Goossens, C. and Berger, A. (1986). Annual and seasonal climatic variations over the northern hemisphere and Europe during the last century. *Ann. Geophys.*, **4(B4)**, 385–400.

Goossens, C. and Berger, A. (1987). How to recognize an abrupt climatic change? In W. H. Berger and L. Labeyrie, editors, *Abrupt Climatic Change, Evidence and Implications*, pages 31–47. D.Reidel Publishing Company, Dordrecht/Boston/Lancaster/Tokyo/, Published in cooperation with NATO Scientific Affairs Division.

Graber, M. A. (1976). Polar motion spectra based upon Doppler, IPMS and BIH data. *Geophys. J. R. astr. Soc.*, **46**, 75–85.

Gross, R. S. (1985). Signal detection techniques applied to the Chandler Wobble. *J. Geophys. Res.*, **90(B12)**, 10281–10290.

Gross, R. S. (1986). The influence of earthquakes on the Chandler wobble during 1977-1983. *Geophys. J. R. astr. Soc.*, **85**, 161–177.

Gross, R. S. (1990). The secular drift of the rotation pole. In Boucher, C., Wilkins, C.A., editor, *Earth Rotation and Coordinate Reference Frames*, pages 146–153. Springer-Verlag, New York.

Guinot, B. (1972). The Chandlerian nutation from 1900 to 1970. *Astron. Astrophys.*, **19**, 207–214.

Guinot, B. (1978). Rotation of the earth and polar motion, services. In *Proc. of the 9th GEOP Conference.*

Guinot, B. (1982). The Chandlerian Nutation from 1900 to 1980. *Geophys. J. R. astr. Soc.*, **71**, 295–301.

Hameed, S. and Currie, R. G. (1989). Simulation of the 14-Month Chandler Wobble in a Global Climate Model. *Geophys. Res. Lett.*, **16(3)**, 247–250.

Haubrich, R. and Munk, W. (1959). The pole tide. *J. Geophys. Res.*, **64**, 2373.

Haubrich, R. A. (1970). An examination of the data relating pole motion to earthquakes. In Mansinha, L., Smylie, D.E., Beck, A.E., editor, *Earthquakes Displacement Fields and the Rotation of the Earth.* Reidel, Dordrecht.

Hide, R. (1984). Rotation of the atmospheres of the Earth and planets. *Phil. Trans. R. Soc. London, Series A*, **313(A1524)**, 107–121.

Jones, P. D., Raper, S. C. B., Bradley, R. S., Diaz, H. F., Kelly, P. M., and Wigley, T. M. L. (1986). Northern hemispheric surface air temperature variations: 1851-1984. *J. Clim. and App. Met.*, **25**, 161–179.

Kanamori, H. (1976). Are earthquakes a major cause of the Chandler wobble? *Nature*, **262**, 254–255.

Kendall, M. and Stuard, A. (1979). *The advanced theory of statistics. Vol. 2 Inference and relationship.* Ch. Griffin and Co. Limited.

Kikuchi, I. and Naito, I. (1982). Sea surface temperature (SST) analyses near the Chandler period. In *Proceedings of the International Latitude Observatory of Mizusawa, No. 21*, volume K, pages 64–70.

Kolaczek, B. (1989). Observational determination of the Earth's rotation. In R. Teisseyre, editor, *Gravity and Low Frequency Geodynamics*, pages 295–361. Elsevier–Warszawa.

Kolaczek, B. and Hua, Y. S. (1991). Astronomical Series of Earth rotation parameters. **177**, 121–138.

Kuehne, J., Wilson, C. R., and Johnson, S. (1996). Estimates of the Chandler wobble frequency and q. *J. Geophys. Res.*, **101**, 13573–13579.

Lambeck, K. (1980). *The Earth's Variable Rotation: Geophysical Causes and Consequences.* Cambridge University Press.

Lambeck, K. (1988). *Geophysical Geodesy - The Slow Deformations of the Earth.* Oxford Science Publications.

Lenhardt, H. and Groten, E. (1985). Chandler wobble parameters from BIH and ILS data. *Manuscripta Geodaetica*, **10**, 296–305.

Maddox, J. (1988). Earthquakes and the Earth's rotation. *Nature*, **332(3)**, 11.

Maksimov, I. V. (1954). On long period tidal phenomena in the sea and in the atmosphere of the earth. *Trans. Inst. Okeanol.*, **8**, 18–40. In Russian.

Maksimov, I. V., Kraklin, V. P., Sarukhanyan, E. I., and Smirnov, N. P. (1967). Nutational migration of the Iceland Low. *Doklady Akademii Nauk SSSR*, **177**(1), 3–6.

Mansinha, L. and Smylie, D. E. (1970). Seismic excitation of the Chandler wobble. In Mansinha, L., Smylie, D.E., Beck, A.E., editor, *Earthquakes Displacement Fields and the Rotation of the Earth*. Reidel, Dordrecht.

Mansinha, L., Smylie, D. E., and Chapman, C. H. (1979). Seismic excitation of the Chandler wobble revisited. *Geophys. J. R. astr. Soc.*, **59**, 1–17.

Merriam, J. B. (1982). Meteorological excitation of the annual polar motion. *Geophys. J. R. astr. Soc.*, **70**, 41–56.

Mulholland, J. R. and Carter, W. E. (1982). Seth Carlo Chandler and the observational origins of geodynamics. In O. Calame, editor, *High-precision Earth rotation and Earth-Moon dynamics, proceedings of the 63rd colloquium of the International Astronomical Union, held at Grasse, France, May 22 - 27, 1981*, pages XV–XIX. D. Reidel Publishing Company, Dordrecht, Boston, London.

Munk, W. H. and MacDonald, G. J. F. (1960). *The Rotation of the Earth*. Cambridge University Press, Cambridge.

Naito, I. (1977). Secular variation of the pole tide. *J. Phys. Earth*, **125**, 221–231.

Newcomb, S. (1891). . *Astron. Jour.*, **11**, 81–83.

Okubo, S. (1982). Is the Chandler period variable? *Geophys. J. R. astr. Soc.*, **71**, 629–646.

Ooe, M. (1978). An optimal complex AR.MA model of the Chandler wobble. *Geophys. J. R. astr. Soc.*, **53**, 445–457.

Pejovič, N. and Vondrák, J. (1991). Polar motion: Observations and atmospheric excitation. Technical report, IUGG Special Study Group 5-98, Bulletin No. 5.

Plag, H.-P. (1988). A regional study of Norwegian coastal long-period sea-level variations and their causes with special emphasis on the Pole Tide. *Berl. Geowiss. Abhandl. Reihe A*, **14**, 1–175.

Plag, H.-P. (1993). The "sea level rise" problem: An assessment of methods and data. In *Proceedings of the International Coastal Congress, Kiel 1992*, pages 714–732. P. Lang Verlag, Frankfurt.

Plag, H.-P. (1995). Coastal relative sea level: A valuable indicator of climate variability? In *XXI General Assembly*, volume Abstracts Week B, page B317. International Union of Geodesy and Geophysics. Abstract.

Preisig, J. R. (1992). Polar motion, atmospheric angular momentum excitation and earthquakes- correlations and significance. *Geophys. J. Int.*, **108(1)**, 161–178.

Runcorn, S. K., Wilkins, G. A., Groten, E., Lenhardt, H., Campbell, J., Hide, R., Chao, B. F., Souriau, A., Hinderer, J., Legros, H., Le Mouel, J.-L., and

Feissel, M. (1988). The excitation of the Chandler Wobble. *Surveys Geophys.*, **9**, 419–449.

Schlesinger, M. E. and Ramankutty, N. (1994). An oscillation in the global climate system of 65-70 years. *Nature*, **367**, 723–726.

Schweydar, W. V. (1916). Die Bewegung der Drehachse der elastischen Erde im Erdkörper und im Raum. *Astron. Nachr.*, **203**, 103–114.

Smith, M. L. (1977). Wobble and nutation of the earth. *Geophys. J. R. astr. Soc.*, **50**, 103–140.

Smylie, D. E. and Mansinha, L. (1971). The elasticity theory of dislocations in real earth Models and changes in the rotation of the Earth. *Geophys. J. R. astr. Soc.*, **23**, 329–354.

Sneyers, R. (1975). Sur l'analyse statistique des séries d'observations. Technical report, Note Technique No. 143, OMM-No. 415, Geneva.

Souriau, A. (1986). Random walk of the Earth's pole related to the Chandler wobble excitation. *Geophys. J. R. astr. Soc.*, **86**, 455–465.

Starr, T. (1983). On the dynamic atmospheric response to the Chandler wobble forcing. *J. Atmos. Sci.*, **40**, 929–940.

Tsimplis, M. N., Flather, R. A., and Vassie, J. M. (1994). The North Sea Pole Tide described through a tide-surge numerical model. *Geophys. Res. Lett.*, **21**, 449–452.

vanDam, T. M., Blewitt, G., and Heflin, M. B. (1994). Atmospheric pressure loading effects on Global Positioning System coordinate determinations. *J. Geophys. Res.*, **99**, 23939–23950.

Vanicek, P. (1970). An analytical technique to minimize noise in a search for lines in the low frequency spectrum. *Observatoire Royal de Belgique, Communications Serie A*, **96**, 170–173.

Volland, H. (1996). Atmosphere and Earth's rotation. *Surveys Geophys.*, **17**, 101–144.

Vondràk, J. (1985). Long-period behaviour of polar motion between 1900.0 and 1984.0. *Ann. Geophys.*, **3(3)**, 351–356.

Wilson, C. R. and Haubrich, R. A. (1976a). Atmospheric contribution to the excitation of the Earth's wobble 1901-1970. *Geophys. J. R. astr. Soc.*, **46**, 745–760.

Wilson, C. R. and Haubrich, R. A. (1976b). Meteorological excitation of the Earth's wobble. *Geophys. J. R. astr. Soc.*, **46**, 707–743.

Wilson, C. R. and Vicente, R. (1980). An analysis of the homogeneous ILS polar motion series. *Geophys. J. R. astr. Soc.*, **62**, 605–616.

Wilson, C. R. and Vicente, R. O. (1990). Maximum likelihood estimates of polar motion parameters. In D. D. McCarthy and W. E. Carter, editors, *Variations in Earth Rotation*, volume 59 of *Geophysical Monograph*, pages 151–155. AGU.

Xie, L. and Dickman, S. R. (1996). Tide gauge analysis of the pole tide in the North Sea. *Geophys. J. Int.*, **126**, 863–870.

Yumi, S. and Yokoyama, K. (1980). Results of the International Latitude Service in a homogenous system 1899.9 – 1979.0. Technical report, Central Bureau of the International Polar Motion Service, Misuzawa.

This article was processed using the LaTeX macro package with LLNCS style